Published in final edited form as:
Circulation. 2008 January 22; 117(3): 388–395. doi:10.1161/CIRCULATIONAHA.107.719765.

Noninvasive in vivo imaging of monocyte trafficking to atherosclerotic lesions

Moritz F. Kircher, MD[1,5], **Jan Grimm, MD, PhD**[1,6], **Filip K. Swirski, PhD**[1,2,4], **Peter Libby, MD**[2,4], **Robert E. Gerszten, MD**[1,3,4], **Jennifer R. Allport, PhD**[1,7], and **Ralph Weissleder, MD, PhD**[1,4,8]

[1]Center for Molecular Imaging Research, Massachusetts General Hospital and Harvard Medical School, Charlestown, MA 02129

[2]Cardiovascular Division, Department of Medicine, Brigham & Women's Hospital and Harvard Medical School, Boston, MA 02115

[3]Cardiovascular Research Center, Massachusetts General Hospital and Harvard Medical School, Charlestown, MA 02129

[4]Donald W. Reynolds Cardiovascular Clinical Research Center on Atherosclerosis at Harvard Medical School

[8]Center for Systems Biology, Massachusetts General Hospital and Harvard Medical School, Boston, MA 02114

Abstract

Background—Monocytes play a key role in atherogenesis, but their participation has been largely discerned via ex vivo analyses of atherosclerotic lesions. We sought to establish a noninvasive technique to determine monocyte trafficking to atherosclerotic lesions in live animals.

Methods and Results—Using a micro-single-photon-emission-computed-tomography (microSPECT/CT) small animal imaging system and an FDA-approved radiotracer ([^{111}Indium] oxyquinoline, ^{111}In-oxine), we demonstrate here that monocyte recruitment to atherosclerotic lesions can be visualized in a noninvasive, dynamic, and three-dimensional fashion in live animals. We demonstrate *in vivo* that monocytes are recruited avidly to plaques within days of adoptive transfer. Using microSPECT/CT imaging as a screening tool, we were able to investigate modulatory effects on monocyte recruitment in live animals. We found that HMG-CoA-reductase inhibitors rapidly and substantially reduce monocyte recruitment to existing atherosclerotic lesions as imaged here *in vivo*.

Conclusions—This novel approach to track monocytes to atherosclerotic plaques *in vivo* should have broad applications and create new insights into the pathogenesis of atherosclerosis and other inflammatory diseases.

Keywords

Imaging; atherosclerosis; plaque; cells

Corresponding author: Ralph Weissleder, MD, PhD, Center for Systems Biology, Massachusetts General Hospital, Richard B. Simches Research Center, 185 Cambridge Street, 8th Floor, Boston, MA 02114, E-mail: rweissleder@mgh.harvard.edu, 617-726-8226 (office), 617-726-5708 (FAX).
[5]Current affiliation: Department of Radiology, Beth Israel Deaconess Medical Center and Harvard Medical School, Boston, MA 02215
[6]Current affiliation: Department of Radiology, Memorial Sloan Kettering Cancer Center, New York, NY 10021
[7]Current affiliation: Novartis Institutes for BioMedical Research Inc., Cambridge, MA 02139

Conflict of Interest Disclosures
None.

Introduction

In the past two decades, the concept of atherogenesis has changed dramatically from the notion of a lipid storage disease to the recognition that inflammation drives this process [1–5]. Substantial evidence identifies monocytes as key cellular participants in the initiation and development of atherosclerotic plaques [5]. Adhesion of monocytes to the arterial endothelium and their migration into the intima occur early in atherogenesis [6]. Monocyte accumulation characterizes fatty streaks, the earliest grossly detectable lesion of human and experimental atherosclerosis [2]. Monocytes differentiate into macrophages [7] and secrete inflammatory cytokines that stimulate smooth muscle cell proliferation and migration [8] and produce proteolytic enzymes that can degrade collagen and render the growing plaque's cap thin and susceptible to rupture [1, 9].

This key role of monocytes in all phases of atherogenesis highlights the need to understand better the dynamics of monocyte recruitment to developing plaques and to develop clinically viable imaging tools to visualize this process in high-risk patient groups or in the development and testing of novel therapies. To date, the data describing monocyte recruitment to atherosclerotic plaques have derived mainly from excised tissue specimens (e.g. in experimental animals, endarterectomy or autopsy samples) that have undergone analysis either histologically [10], by polymerase chain reaction methods [11, 12], or by flow cytometry [7]. Thus, the analysis of monocyte trafficking to lesions has often been restricted to a static view that does not reflect the dynamics of this process. The ability to assess recruitment of monocytes *in vivo* would benefit in advancing our understanding of atherogenesis, evaluating anti-inflammatory drugs designed to inhibit monocyte recruitment, and stratifying patients at risk for developing complications of atherosclerosis.

Here we present an approach that enables non-invasive, dynamic, quantitative and high-resolution *in vivo* imaging of monocyte trafficking to atherosclerotic lesions. We demonstrate the feasibility of detection of the recruitment of monocytes labeled with [^{111}Indium] oxyquinoline (^{111}In-oxine) to existing atherosclerotic lesions of apolipoprotein E-deficient (ApoE−/−) mice by micro-single-photon-emission-computed-tomography/CT (microSPECT/CT). The long half-life of ^{111}In (2.8 days) enabled the detection of monocytes for up to 7 days after adoptive transfer, and the high-resolution anatomical data derived from CT allowed localization of hotspots of monocyte infiltration in a sub-millimeter range. Furthermore we demonstrate that microSPECT/CT imaging allows for assessing the effect of an intervention (statin drugs) on monocyte recruitment to plaques *in vivo*. This technique may open new avenues to investigate non-invasively the mechanisms of atherogenesis and other inflammatory diseases and to evaluate effectively new anti-inflammatory therapies. Importantly, with both human SPECT/CT scanners and the FDA-approved ^{111}In-oxine in clinical use, our results support the potential to conduct similar studies in humans in the future.

Methods

Materials

RPMI 1640, HBSS and FBS were purchased from Cellgro (Herndon, VA). PBS was obtained from BioWhittaker (Walkersville, MD). [^{111}Indium] Oxyquinoline (^{111}In-oxine) was purchased from Amersham-GE (Piscataway, NJ). Ultravist™ iodinated contrast agent for CT imaging was obtained from Berlex (Richmond, CA).

Antibodies

The primary polyclonal anti-GFP antibody was purchased from Chemicon International (Temecula, CA; cat# AB3080).

Animals

ApoE−/− mice (B6.129P2-*Apoe*^{tm1Unc}), EGFP expressing (C57BL/6-Tg(ACTB-EGFP)1Osb/J) mice, and C57BL/6 mice (6–8 wk old) were purchased from Jackson Laboratories (Bar Harbor, ME). The ApoE−/− animals had been backcrossed to the C57BL/6 background for at least ten generations. Mice were cared for according to the Institution's animal facility guidelines. At 4 wk of age, ApoE−/− animals were placed on a Western diet (42% adjusted caloric diet, 0.2% cholesterol, Harlan Teklad) and fed until use for experiments. The remaining animals remained on a regular chow diet. All protocols were approved by the Animal Review Committee.

Statin treatment

ApoE−/− animals in the treatment group received simvastatin (oral, 0.57 mg $kg^{-1}d^{-1}$, Zocor®, Merck) and atorvastatin (oral, 0.57 mg $kg^{-1}d^{-1}$; Lipitor®, Pfizer) dissolved in 100 μl PBS via intragastric instillation x 3 days p.o. (0.57 mg kg^{-1} corresponds to a 40 mg dose used clinically in humans (70 kg body weight); recommended atorvastatin dose in humans is 10–80 mg d^{-1}). Mevastatin (Sigma) was administered s.q. (20 mg $kg^{-1}d^{-1}$, according to [13]) dissolved in 20 μl PBS. Control animals received PBS only via intragastric or s.c. instillation, respectively.

Measurement of cholesterol levels

Total blood cholesterol levels of atorvastatin-treated mice and non-treated control mice were measured with a Raichem (San Diego, CA) cholesterol reagent kit according to the protocol of the manufacturer.

Monocyte isolation

We employed a two-step combination of density gradient separation and negative immunomagnetic depletion to isolate murine monocytes from the peripheral blood, as described in [14] with minor modifications. In brief, peripheral blood (1–1.3 ml) was drawn from C57BL/6 mice (typically n=15 mice/isolation) via cardiac puncture, diluted 5:1 with HBSS, and subjected to density centrifugation (30 min, 1600 rpm, RT) over Histopaque-1083 (Sigma). The buffy coat containing peripheral blood mononuclear cells (PBMCs) was aspirated, washed 3 x in HBSS and subsequently washed 1x in MACS-Buffer (PBS containing 0.1% (w/v) BSA and 0.5mM EDTA). T cells, B cells and NK cells were depleted from the PBMC population using a cocktail of immunomagnetic beads (anti-CD90, anti-CD45R and anti-CD49b beads (Miltenyi Biotec, Auburn, CA). Monocyte purity was determined by morphologic analysis of cells prepared by cytospin and Wright-Giemsa staining as well as independently via FACS analysis.

Monocyte labeling, viability and function

Labeling: Purified monocytes were labeled with ^{111}In-oxine according to the manufacturer's protocol (Amersham Health Medi-Physics, Arlington Heights, IL). Briefly, cells were washed with HBSS, spun and resuspended in ^{111}In-oxine for 20 min at 37°C, pH 6.5–7.5. The cells were then washed 3x with HBSS. *Viability*: Potential cytotoxic effects of ^{111}In-oxine on monocyte viability were assessed by Trypan blue exclusion staining. *Function*: We employed a model of thioglycollate-induced sterile peritonitis modified after Segal et al [15]. Sterile thioglycollate medium (1 ml) was injected i.p. into C57BL/6 mice (n=3). After 24 hours, 3 × 10^6 monocytes were isolated as described and divided into two batches. Batch 1 was labeled

with ^{111}In-oxine (5pCi/cell) and subsequently co-labeled with the Indocyanine dye DiO (Molecular Probes). Batch 2 was incubated with PBS only and subsequently labeled with the dye DiD (Molecular Probes). Batch 1 and 2 were then mixed together and 10^6 cells of the mixture injected via tail vein into each of the three recipient mice with peritonitis. Again 24 hours later, animals were sacrificed and peritoneal lavages performed. The recovered cells were analyzed via FACS analysis in FL1 channel (to detect DiO+/^{111}In-oxine-labeled monocytes) and FL4 channel (to detect DiD+/mock-labeled monocytes).

MicroSPECT/CT imaging and post-processing

For *in vivo* SPECT/CT imaging, monocytes were isolated as described and labeled with ^{111}In-oxine. For selected experiments, PBMCs or PBMCs without monocytes (termed "PBMC^{-monos}") were also used for experiments. Recipient ApoE$^{-/-}$ or C57BL/6 wild-type mice, respectively, were placed under general isoflurane inhalation anesthesia and 3×10^6 cells were injected via tail vein. The total amount of activity injected into each animal was measured with a radioisotope calibrator (Capintec, Ramsey, NJ) immediately after injection and before imaging time-points to account for differences in injected/excreted activity. SPECT/CT imaging was performed with an integrated high-resolution micro-SPECT/CT imaging system (X-SPECT; Gamma Medica Inc., Northridge, CA), which combines SPECT and CT on one gantry, allowing for immediate coregistration of the SPECT and CT datasets by the scanner software without additional postprocessing. For imaging, mice were anesthetized using isoflurane inhalation, with parameters set so that the animals were breathing shallow to reduce artifacts from respiratory movements. The animals were scanned repeatedly from 30 min. post injection to up to 10 days after adoptive transfer. For quantitative analysis an imaging time-point of 5 days was used, as activity in the blood interfering with the results was negligible by this time. Average imaging time was 30 min. and was adjusted when needed to correct for differences in activity between animals.

Ultravist – 300 was injected via pump (60 μl/min.) over the 10 minute CT scans for vascular contrast. In select experiments, animals were sacrificed and contrast was infused via syringe into the left ventricle. The ascending aorta, aortic arch, descending (thoracic) aorta and descending (abdominal) aorta, were segmented out along with muscle background using the contrast enhanced CT images using Amira® software (Mercury Computer Systems, Inc.). The ROI (regions of interests) from the CT images were propagated to the registered SPECT images and the mean value of each ROI was tabulated. These mean values of each aortic ROI were divided by the mean muscle ROI to give a signal to noise ratio. 3D rendering was performed with Amira software on a high-end PC workstation.

Autoradiography

Mice were sacrificed and aortas excised and exposed on a Phosphorimager SI (Molecular Dynamics, Sunnyvale, CA) for 24h. ^{111}In-oxine standards were exposed together with the specimen on the same plate, allowing for calibration and quantitative data analysis by region of interest analysis using ImageJ (NIH) as described [16]. Background activity measured in C57BL/6 mice was subtracted from the activity measured in ApoE$^{-/-}$ mice.

Immunohistochemistry

Monocytes were isolated from EGFP expressing mice (The Jackson Laboratory) and adoptively transferred into 20-wk-old ApoE−/− mice. EGFP was used for its antigenic, rather than fluorescent properties. Five days after transfer, animals were sacrificed and aortas excised, frozen in OCT and cut into 5 μm sections in a cryostat. After sections were dried at room temperature for 20 minutes, they were treated with 0.3 % hydrogen peroxide to inhibit endogenous peroxidase activity and incubated for 30 minutes in blocking solution. Adjacent sections were then incubated with primary polyclonal anti-GFP (Chemicon cat# AB3080) or

rat anti-mouse Mac-3 antibodies diluted in PBS supplemented with 4% of the species-respective normal serum (GFP 1:25; Mac-3 1:50). After washing with PBS, species-appropriate secondary antibodies were applied, followed by avidin-peroxidase complex (Vectastain ABC kit; Vector Laboratories). Slides were rinsed in PBS after each incubation step. The reaction was visualized with 3-amino-9-ethyl carbazole substrate (AEC; Sigma). Sections were counterstained with Gill's hematoxylin solution (Sigma) and mounted.

Statistical Methods

To test for differences between treatment groups, one-way ANOVA with Tukey's Multiple Comparison Test was computed using Graphpad Prism. The authors point out that with small sample sizes and an unbalanced design, the data may not meet ANOVA assumptions and therefore caution is required in interpretation. To test for correlation between monocyte numbers and SPECT signal, Pearson's product-moment correlation coefficient was calculated using Excel.

The authors had full access to the data and take responsibility for its integrity. All authors have read and agree to the manuscript as written.

Results

Monocyte Isolation and effect of ^{111}In-oxine labeling on monocyte function

We isolated total murine monocytes using a recently described 2-step negative depletion method [14]. Fig. 1A shows representative morphological examples of eluates containing monocytes and the fraction depleted during magnetic separation. Monocyte purity was typically > 90% (90.8 ± 3.0, mean ± SD) with most contaminating cells being lymphocytes (7.4 ± 0.9 %). Correspondingly, the fraction containing the magnetically depleted cells contained mostly lymphocytes (92.2 ± 4.9) (Fig. 1B).

Labeling of monocytes with ^{111}In-oxine did not affect their overall viability, as shown by Trypan Blue exclusion staining (Fig. 1C). Determination of a potential effect of ^{111}In-oxine on the migratory capability of monocytes *in vivo* employed cell migration to the peritoneal cavity. We tagged ^{111}In-oxine labeled vs. non-labeled monocytes with different cell-tracker dyes, injected a 1:1 mixture intravenously to mice with thioglycollate-induced peritonitis, and assessed the number of monocytes that accumulated in the peritoneal cavity. Monocytes accumulated in the peritoneum, and there was no statistical difference between ^{111}In-oxine-labeled and non-labeled cells (Fig. 1D).

Non-invasive imaging of monocyte trafficking to atherosclerotic plaques by micro-SPECT/CT

Initial *in vivo* experiments used monocytes isolated from the peripheral blood (n=15) of C57BL/6 wildtype donor mice and adoptively transferred 3×10^6 monocytes to recipient mice. We serially imaged the recipient animals from 30 min. until 10 days following the adoptive transfer to determine the timeline for redistribution of monocytes (Fig 1E, and data not shown). Within the first day (0 – 24h) a positive signal, corresponding to labeled monocytes, was detected in heart and lungs. After 36 h, monocyte distribution had shifted towards liver and spleen, with less activity seen in the heart and lungs. At the 5 day time-point, there was no residual activity in the heart and lungs and a focal hotspot in the ascending aorta now appeared. Histological analysis showed that areas of SPECT/CT activity corresponded to areas of abundant monocyte recruitment. As murine monocytes do not express a distinct marker that allows for specific antibody staining, GFP expressing monocytes were transferred in these experiments to allow for detection with anti-GFP antibodies (Fig. 1F). The 5-day time-point was used in the remaining experiments, as it allows for detection of sufficient remaining

radioactive signal while minimizing background signal from monocytes in the circulation. We next tested whether the signal detected in aortas was specific for monocytes (Fig. 2). We transferred either monocytes or peripheral blood mononuclear cells (PBMCs) that did not contain monocytes (depleted fraction during negative isolation) into $ApoE^{-/-}$ mice. A second control used injection of monocytes into C57/BL6 wildtype mice. As shown in the CT (Fig. 2A) and SPECT/CT overlays (Fig. 2B) ^{111}In-oxine labeled monocytes are recruited to the ascending part of the aorta of $ApoE^{-/-}$ mice. Other parts of the central arterial tree do not show substantial monocyte recruitment. Autoradiography of excised aortas verified the localized recruitment to the ascending aorta (Fig. 2C). In contrast, neither PBMCs depleted of monocytes (consisting mainly of T- and B-lymphocytes) injected into $ApoE^{-/-}$ mice, nor monocytes injected into C57BL/6 wild-type mice demonstrated substantial recruitment to the aorta. Magnified views and 3D rendering of the 2D SPECT/CT dataset of monocyte transfer into $ApoE^{-/-}$ mice is shown in Fig. 3 and in the accompanying web-movie (supplemental data).

To investigate the relationship between the *in vivo* SPECT signal and the actual numbers of ^{111}Indium-labeled monocytes in the aortas, we estimated monocyte numbers based on autoradiography data of excised aortas obtained after performance of *in vivo* SPECT imaging. The analysis showed a strong linear correlation between the *in vivo* SPECT signal and the monocyte content, with an R^2 of 0.87 (supplemental Figure).

Statin treatment of $ApoE^{-/-}$ mice rapidly reduces acute monocyte recruitment to existing plaque

Having established SPECT/CT imaging as a tool to assess cellular recruitment to atherosclerotic lesions, we extended our studies to investigate whether a therapeutic intervention could modulate the imaging signal *in vivo*. Statin treatment can reduce the total number of macrophages in murine plaques after 6 months of treatment [17]. However, the static nature of the study did not address the question of mechanism of action, and if the statin directly effected monocyte recruitment. Thus, further experiments evaluated *in vivo* the effect of mevastatin, simvastatin, or atorvastatin on monocyte recruitment to atheromata. We assessed whether statins affected monocyte recruitment, and therefore chose to treat recipient animals for only three days (1 dose/day) before cells were injected. *In vivo* microSPECT/CT imaging revealed an approx. 5-fold reduction in monocyte recruitment to plaques when compared to placebo-treated mice ($p < 0.001$) (Fig. 4). All three statins examined had similar effects on the reduction of monocyte recruitment (Fig. 4). Cholesterol levels between untreated and atorvastatin-treated animals showed no statistically significant difference (data not shown).

To corroborate the effect observed during *in vivo* screening, we then examined the effect of statin on monocyte recruitment with an independent method. Animals were sacrificed, aortas excised and recruitment quantified by autoradiography. This approach demonstrated an approx. 10-fold reduction in monocyte recruitment in statin-treated mice ($p < 0.001$; Fig. 5). To test if the statin effect would act on the site of the vessel wall, or on the monocytes themselves, we treated the donor mice, while leaving the recipient mice untreated. The untreated and treated group did not differ significantly, suggesting that statin does not act on the monocytes but rather on the vessel wall to reduce trafficking under the conditions of these experiments (Fig. 5).

Discussion

We report here that monocyte recruitment to plaques can be assessed by microSPECT/CT imaging and thus be visualized in a non-invasive, dynamic, three-dimensional and quantitative fashion. The long half-life of radiotracer isotopes available for SPECT imaging enables repetitive imaging of monocyte biodistribution in the same animal, tracking its migration from circulation to atherosclerotic lesions.

Previous reports have indicated that lesion macrophage content may be gauged by magnetic resonance imaging (MRI) [18, 19], optical coherence tomography (OCT) [20] or computed tomography (CT) [21]. However, these methods can only describe the total number of resident macrophages or overall metabolic activity, respectively, in a plaque at a given time. As atherogenesis is a chronic and dynamic process, the number of macrophages present in a plaque at a given time is the combined result of monocyte recruitment, differentiation, death, and efflux from the plaque. The same limitation holds true for positron-emission-tomography (PET) studies using fluorodeoxyglucose (FDG), which have shown promise in estimating the overall degree of vascular inflammation [22, 23]. In contrast to these techniques, *in vivo* SPECT/CT imaging now enables assessment of monocyte accumulation serially in the same animal, allowing a much more direct study of factors that modulate recruitment.

The method we describe here has several limitations. The resolution of the present approach is lower compared to certain high-resolution modalities such as MRI. Coregistration with CT (as in the current study) and in the future also MRI can reduce this shortcoming by providing greater anatomical detail and hence better spatial localization of the tracer signal.

SPECT/CT imaging of adoptively transferred cells measures the total number of gamma photons in a defined three-dimensional space and assumes an equal number of photons emitted from each cell. The method may underestimate the number of recruited cells as they undergo apoptosis, which may lead to loss of tracer. The known progressive loss of ^{111}In over time in healthy cells is relatively constant, although some variations may occur in vivo in different disease models. Indium that has lost its association with cells does not significantly influence the local, cell bound activity as our prior studies have shown that free ^{111}In is rapidly excreted through the kidneys [14].

A confounding variable in the interpretation of the results is the possibility that monocytes turn over in atherosclerotic plaques due to continued recruitment and emigration. However, the data of Llodra et al. have shown that while this is true for wild-type mice, there is only minimal emigration of monocytes from plaques in ApoE$^{-/-}$ mice [24]. Based on this data we believe that the signal detected in lesions in our study reflects the accumulation of monocytes over the 5-day period from adoptive transfer until the imaging endpoint. We understand that the number of adoptively transferred monocytes (3×10^6) exceeded the number of circulating monocytes in the recipient animal, which may affect the rate of monocyte trafficking, particularly in the initial hours/days.

Several technical factors were crucial to the development of a robust imaging technique. As monocytes occur in relatively small numbers in the peripheral blood of mice and do not express a known unique surface marker, their isolation represents a challenge. Here we employed a two-step method, recently described and characterized in more detail [14], that allows high-purity isolation while preserving cell viability and functionality.

Prerequisites for a suitable radioactive tracer used to label monocytes include ready availability, negligible cytotoxic effects, sufficient labeling efficiency, and a long half-life. The radiotracer compound ^{111}In-oxine used here is available in a form ready for coincubation with cells, and is approved by the FDA for labeling autologous leukocytes. Despite extensive testing in vitro and *in vivo*, we did not find adverse effects on viability or function of monocytes.

^{111}In-oxine has a physical half-life ($t_{1/2}$ = 2.8 days) that is significantly longer than isotopes available for positron-emission-tomography (PET) imaging, such as ^{64}Cu (12.7 h) or ^{18}F (110 min) [25]. This translated in our ability to visualize monocyte trafficking by microSPECT/CT for up to 7–10 days, whereas the longest cell-tracking periods possible with state-of-the-art PET imaging have been reported to be 24–36 h [25] except for HSV-tk techniques which require genetic modification of cells. This property has particular importance to the present study, as

we were able to use a delayed imaging time-point (5 days) for the readout, avoiding detection of false positive signal derived from circulating monocytes (We had recently determined the half-life of circulating blood monocytes in mice to be 43.5 ± 7.9 h, corresponding to a 95% monocyte clearance from the circulation at the time-point of 5 days after injection [14]).

The SPECT signal localized predominantly in regions of the ascending aorta, the site of the largest plaques in the majority of animals, while certain small lesions did not emit detectable signal. This observation may result from lesion heterogeneity, i.e. some lesions may be more active than others. This method may therefore be used to identify lesions that are recruiting more monocytes. Alternatively, the total number of cells in smaller lesions is below the SPECT detection threshold. Further improvement of labeling efficiency and improvement in SPECT technology should increase sensitivity in the future.

Having an *in vivo* imaging system at hand, we could then use it to assess efficiently the effect of modulating factors on monocyte recruitment, avoiding labor-intensive ex vivo procedures.

All three tested statins had an acute effect on monocyte recruitment, rapidly and independently of significant effects on plasma cholesterol levels. To our knowledge this is the first time that such acute statin effects have been reported. Prospective clinical trials have convincingly demonstrated that statins can effectively lower the incidence of cardiovascular events in primary and secondary prevention [26]. An increasing body of evidence suggests that statins cause these clinical benefits in part by anti-inflammatory effects not directly related to the lowering of LDL cholesterol (LDL-C), a hypothesis supported by the present observations. Statin-induced alterations in arterial biology that may not depend on cholesterol lowering include reduction in the expression of factors involved in the recruitment of inflammatory cells, such as MCP-1 [17, 27], ICAM-1 [26], IL-6 and IL-8 [28], TNF-α [17] and NF-κB activity [27] and monocytosis [7]. Several reviews point to uncertainty regarding the *in vivo* relevance of such "pleiotropic" effects [26, 29]. Recent analyses of clinical trials however support the concept that an important component of statins' reduction in recurrent cardiovascular events does not depend on LDL reduction [30, 31]. The relevance of LDL-independent effects of statins also remains unclear because many in vitro studies used statin concentrations too high to have clinical relevance [29]. Most of the studies in mice used dosages between 10–30 mg/kg [32, 33], which is at least an order of magnitude higher than the clinically prescribed range of 10–80 mg/person/day (0.14 – 1.14 mg/kg for a standard weight of 70 kg). The atorvastatin dosage used here (0.57 mg/kg) corresponds to a 40 mg dose in humans. The current study - using a low dose - showed that atorvastatin causes an immediate and substantial reduction in monocyte recruitment to atherosclerotic plaques. After treating $ApoE^{-/-}$ mice with only three statin doses, the monocyte recruitment to plaques fell 5-fold *in vivo*. This finding has considerable importance, as it highlights the potential of statins to suppress a key step in atherogenesis via an effect independent of LDL-C lowering. Furthermore, it supports the relevance of previous in vitro reports on the effect of statins on mediators of monocyte attachment to and transmigration through the vascular endothelium. Reciprocal experiments treated the donor mice (and therefore exposed the monocytes to atorvastatin but not the vessel wall of the recipients) and showed no significant reduction in monocyte recruitment. This finding suggests that atorvastatin reduces recruitment by acting at the level of the arterial wall rather than on the monocytes themselves. However, the possibility remains that the statin effect on monocytes in vivo may have been lost during monocyte isolation and no longer operate upon adoptive transfer. Therefore we cannot conclude that statins affect exclusively the vascular wall under these conditions.

In summary, we present novel mechanistic insight into monocyte accumulation in atheromata, and the anti-inflammatory action of statins, using a new tool that permits tracking of cells to the vascular wall noninvasively *in vivo*. Using monocytes in the context of atherogenesis, we

exemplify how this technique can be applied to elucidate important biological events. As the key components of the technique are in clinical use, its application to human patients may be within reach.

Supplementary Material

Refer to Web version on PubMed Central for supplementary material.

Acknowledgments

We thank Gregory Wojtkiewicz and Pratik Patel for assistance with data analysis and image postprocessing, Dr. Elena Aikawa for performing immunohistochemistry, and Dr. Emerson Liu for technical advice. We also acknowledge Dr. Mikael Pittet for critical review of the manuscript and Drs. Farouc Jaffer and Matthias Nahrendorf for helpful discussions.

Sources of Funding

This work was supported, in part, by NIH grants U01 HL080731 and R24 CA92782 (both to R.W.), the Donald W. Reynolds Cardiovascular Clinical Research Center on Atherosclerosis at Harvard Medical School (to P.L. and R.W.), the American Heart Association (both M.F.K. and F.K.S. are recipients of American Heart Association Postdoctoral Fellowship Awards) and a seed grant from the Radiological Society of North America (to J.G.).

References

1. Li AC, Glass CK. The macrophage foam cell as a target for therapeutic intervention. Nat Med 2002;8:1235–1242. [PubMed: 12411950]
2. Libby P. Inflammation in atherosclerosis. Nature 2002;420:868–874. [PubMed: 12490960]
3. Binder CJ, Chang MK, Shaw PX, Miller YI, Hartvigsen K, Dewan A, Witztum JL. Innate and acquired immunity in atherogenesis. Nat Med 2002;8:1218–1226. [PubMed: 12411948]
4. Libby P, Ridker PM. Inflammation and atherosclerosis: role of C-reactive protein in risk assessment. Am J Med 2004;116(Suppl 6A):9S–16S. [PubMed: 15050187]
5. Ross R. Atherosclerosis--an inflammatory disease. N Engl J Med 1999;340:115–126. [PubMed: 9887164]
6. Sanz J, Moreno PR, Fuster V. Update on advances in atherothrombosis. Nat Clin Pract Cardiovasc Med 2007;4:78–89. [PubMed: 17245402]
7. Swirski FK, Libby P, Aikawa E, Alcaide P, Luscinskas FW, Weissleder R, Pittet MJ. Ly-6C monocytes dominate hypercholesterolemia-associated monocytosis and give rise to macrophages in atheromata. J Clin Invest 2007;117:195–205. [PubMed: 17200719]
8. Libby P, Ridker PM, Maseri A. Inflammation and atherosclerosis. Circulation 2002;105:1135–1143. [PubMed: 11877368]
9. Libby P. Current concepts of the pathogenesis of the acute coronary syndromes. Circulation 2001;104:365–372. [PubMed: 11457759]
10. Lessner SM, Prado HL, Waller EK, Galis ZS. Atherosclerotic lesions grow through recruitment and proliferation of circulating monocytes in a murine model. Am J Pathol 2002;160:2145–2155. [PubMed: 12057918]
11. Kim CJ, Khoo JC, Gillotte-Taylor K, Li A, Palinski W, Glass CK, Steinberg D. Polymerase chain reaction-based method for quantifying recruitment of monocytes to mouse atherosclerotic lesions in vivo: enhancement by tumor necrosis factor-alpha and interleukin-1 beta. Arterioscler Thromb Vasc Biol 2000;20:1976–1982. [PubMed: 10938020]
12. Steinberg D, Khoo JC, Glass CK, Palinski W, Almazan F. A new approach to determining the rates of recruitment of circulating leukocytes into tissues: application to the measurement of leukocyte recruitment into atherosclerotic lesions. Proc Natl Acad Sci U S A 1997;94:4040–4044. [PubMed: 9108101]
13. Budzyn K, Marley PD, Sobey CG. Chronic mevastatin modulates receptor-dependent vascular contraction in eNOS-deficient mice. Am J Physiol Regul Integr Comp Physiol 2004;287:R342–R348. [PubMed: 15130878]

14. Swirski FK, Pittet MJ, Kircher MF, Aikawa E, Jaffer FA, Libby P, Weissleder R. Monocyte accumulation in mouse atherogenesis is progressive and proportional to extent of disease. Proc Natl Acad Sci U S A 2006;103:10340–10345. [PubMed: 16801531]
15. Segal BH, Kuhns DB, Ding L, Gallin JI, Holland SM. Thioglycollate peritonitis in mice lacking C5, 5-lipoxygenase, or p47(phox): complement, leukotrienes, and reactive oxidants in acute inflammation. J Leukoc Biol 2002;71:410–416. [PubMed: 11867678]
16. Kircher MF, Allport JR, Graves EE, Love V, Josephson L, Lichtman AH, Weissleder R. In vivo high resolution three-dimensional imaging of antigen-specific cytotoxic T-lymphocyte trafficking to tumors. Cancer Res 2003;63:6838–6846. [PubMed: 14583481]
17. Kleemann R, Princen HM, Emeis JJ, Jukema JW, Fontijn RD, Horrevoets AJ, Kooistra T, Havekes LM. Rosuvastatin reduces atherosclerosis development beyond and independent of its plasma cholesterol-lowering effect in APOE*3-Leiden transgenic mice: evidence for antiinflammatory effects of rosuvastatin. Circulation 2003;108:1368–1374. [PubMed: 12939225]
18. Amirbekian V, Lipinski MJ, Briley-Saebo KC, Amirbekian S, Aguinaldo JG, Weinreb DB, Vucic E, Frias JC, Hyafil F, Mani V, Fisher EA, Fayad ZA. Detecting and assessing macrophages in vivo to evaluate atherosclerosis noninvasively using molecular MRI. Proc Natl Acad Sci U S A 2007;104:961–966. [PubMed: 17215360]
19. Ruehm SG, Corot C, Vogt P, Kolb S, Debatin JF. Magnetic resonance imaging of atherosclerotic plaque with ultrasmall superparamagnetic particles of iron oxide in hyperlipidemic rabbits. Circulation 2001;103:415–422. [PubMed: 11157694]
20. Tearney GJ, Yabushita H, Houser SL, Aretz HT, Jang IK, Schlendorf KH, Kauffman CR, Shishkov M, Halpern EF, Bouma BE. Quantification of macrophage content in atherosclerotic plaques by optical coherence tomography. Circulation 2003;107:113–119. [PubMed: 12515752]
21. Hyafil F, Cornily JC, Feig JE, Gordon R, Vucic E, Amirbekian V, Fisher EA, Fuster V, Feldman LJ, Fayad ZA. Noninvasive detection of macrophages using a nanoparticulate contrast agent for computed tomography. Nat Med 2007;13:636–641. [PubMed: 17417649]
22. Bural GG, Torigian DA, Chamroonrat W, Alkhawaldeh K, Houseni M, El-Haddad G, Alavi A. Quantitative assessment of the atherosclerotic burden of the aorta by combined FDG-PET and CT image analysis: a new concept. Nucl Med Biol 2006;33:1037–1043. [PubMed: 17127178]
23. Elmaleh DR, Fischman AJ, Tawakol A, Zhu A, Shoup TM, Hoffmann U, Brownell AL, Zamecnik PC. Detection of inflamed atherosclerotic lesions with diadenosine-5′,5‴-P1,P4-tetraphosphate (Ap4A) and positron-emission tomography. Proc Natl Acad Sci U S A 2006;103:15992–15996. [PubMed: 17038498]
24. Llodra J, Angeli V, Liu J, Trogan E, Fisher EA, Randolph GJ. Emigration of monocyte-derived cells from atherosclerotic lesions characterizes regressive, but not progressive, plaques. Proc Natl Acad Sci U S A 2004;101:11779–11784. [PubMed: 15280540]
25. Adonai N, Nguyen KN, Walsh J, Iyer M, Toyokuni T, Phelps ME, McCarthy T, McCarthy DW, Gambhir SS. Ex vivo cell labeling with 64Cu-pyruvaldehyde-bis(N4-methylthiosemicarbazone) for imaging cell trafficking in mice with positron-emission tomography. Proc Natl Acad Sci U S A 2002;99:3030–3035. [PubMed: 11867752]
26. Wolfrum S, Jensen KS, Liao JK. Endothelium-dependent effects of statins. Arterioscler Thromb Vasc Biol 2003;23:729–736. [PubMed: 12615672]
27. Bustos C, Hernandez-Presa MA, Ortego M, Tunon J, Ortega L, Perez F, Diaz C, Hernandez G, Egido J. HMG-CoA reductase inhibition by atorvastatin reduces neointimal inflammation in a rabbit model of atherosclerosis. J Am Coll Cardiol 1998;32:2057–2064. [PubMed: 9857893]
28. Rezaie-Majd A, Maca T, Bucek RA, Valent P, Muller MR, Husslein P, Kashanipour A, Minar E, Baghestanian M. Simvastatin reduces expression of cytokines interleukin-6, interleukin-8, and monocyte chemoattractant protein-1 in circulating monocytes from hypercholesterolemic patients. Arterioscler Thromb Vasc Biol 2002;22:1194–1199. [PubMed: 12117737]
29. Libby P, Aikawa M. Mechanisms of plaque stabilization with statins. Am J Cardiol 2003;91:4B–8B.
30. Morrow DA, de Lemos JA, Sabatine MS, Wiviott SD, Blazing MA, Shui A, Rifai N, Califf RM, Braunwald E. Clinical relevance of C-reactive protein during follow-up of patients with acute coronary syndromes in the Aggrastat-to-Zocor Trial. Circulation 2006;114:281–288. [PubMed: 16847150]

31. Ridker PM, Cannon CP, Morrow D, Rifai N, Rose LM, McCabe CH, Pfeffer MA, Braunwald E. C-reactive protein levels and outcomes after statin therapy. N Engl J Med 2005;352:20–28. [PubMed: 15635109]

32. Nachtigal P, Jamborova G, Pospisilova N, Pospechova K, Solichova D, Zdansky P, Semecky V. Atorvastatin has distinct effects on endothelial markers in different mouse models of atherosclerosis. J Pharm Pharm Sci 2006;9:222–230. [PubMed: 16959191]

33. Suzuki M, Kakuta H, Takahashi A, Shimano H, Tada-Iida K, Yokoo T, Kihara R, Yamada N. Effects of atorvastatin on glucose metabolism and insulin resistance in KK/Ay mice. J Atheroscler Thromb 2005;12:77–84. [PubMed: 15942117]

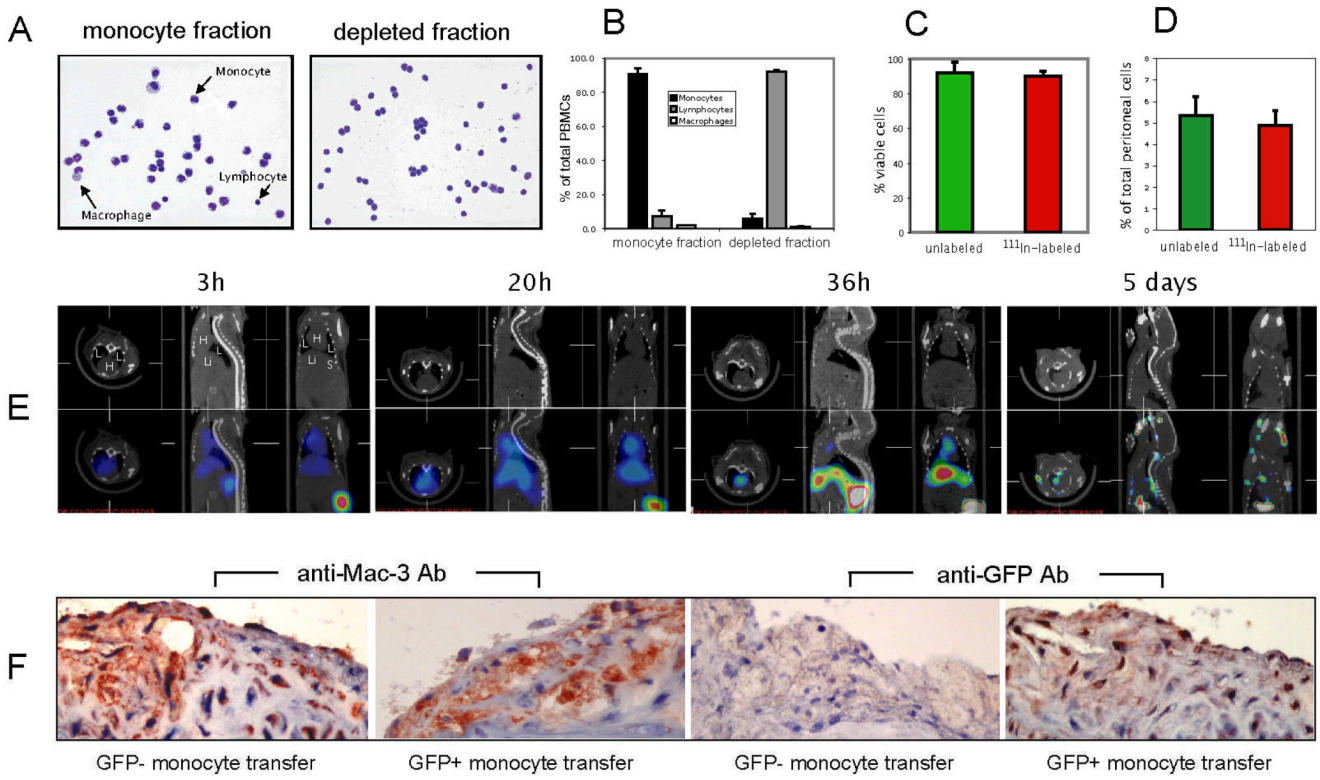

Figure 1. Characterization of monocyte isolation, effect of ^{111}In-oxine labeling on monocyte function, *in vivo* biodistribution and histological validation

A, Cytospin and Wright-Giemsa staining of monocyte fraction and depleted fraction of PBMCs. **B**, Quantification of monocyte purity based on manual counting of cytospin slides (summary of three independent experiments). **C**, Effect of ^{111}In-oxine labeling on monocyte viability as determined by Trypan blue staining. **D**, Effect of ^{111}In-oxine labeling on the *in vivo* recruitment capability of monocytes in a model of thioglycollate-induced peritonitis. **E**, *In vivo* SPECT/CT imaging time-course of monocyte biodistribution in ApoE$^{-/-}$ mouse (H = heart; L = lung; Li = liver; S = spleen). **F**, Histological validation of monocyte recruitment to atherosclerotic plaques in ApoE$^{-/-}$ mice 5 days after injection of GFP− or GFP+ monocytes, respectively. Immunohistochemistry using Abs against Mac-3 and GFP (sister sections; positive staining for both in red (note the positive staining in all sections except for anti-GFP staining with transfer of GFP- monocytes). Data are representative of three independent experiments.

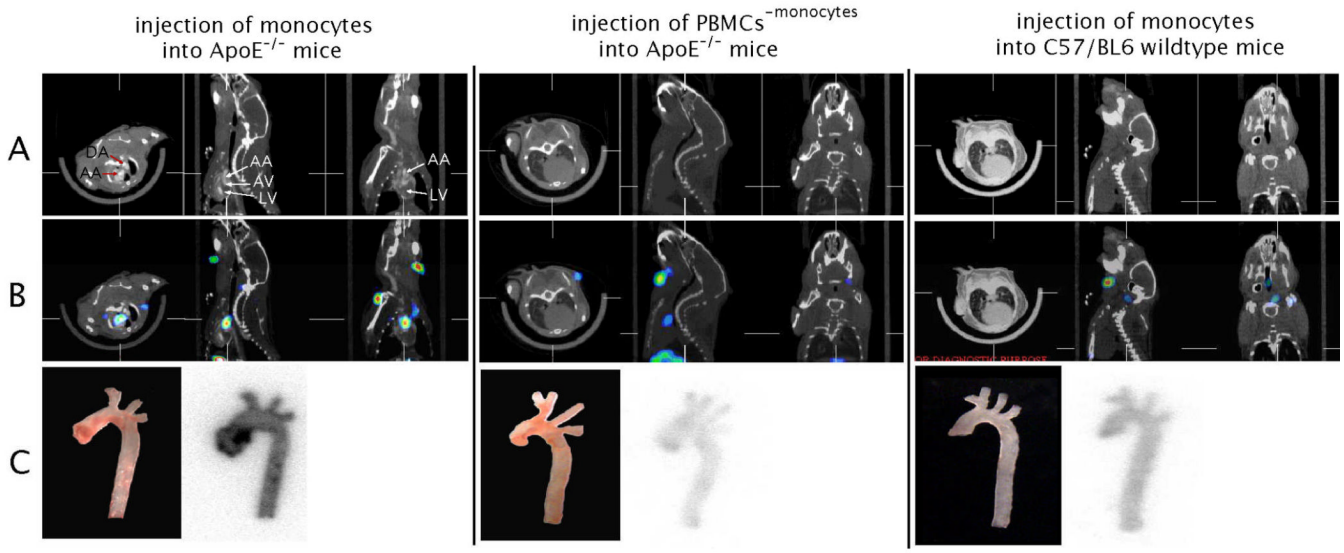

Figure 2. microSPECT/CT allows imaging of monocyte recruitment to atherosclerotic plaques

Monocytes vs. PBMCs without monocytes (PBMC$^{-monocytes}$) were labeled with ^{111}In-oxine and transferred into ApoE$^{-/-}$ mice (left, middle). As a control, monocytes were transferred into C57BL/6 wildtype mice (right). MicroSPECT/CT imaging was performed 5 days after injection of cells. **A** CT images in axial, sagittal and coronal views, respectively. **B**, SPECT/CT overlay images in axial, sagittal and coronal views, respectively. **C** white light images and corresponding autoradiography exposures of aortas excised after *in vivo* imaging. (LV = left ventricle; AV = aortic valve region; AA = ascending aorta).

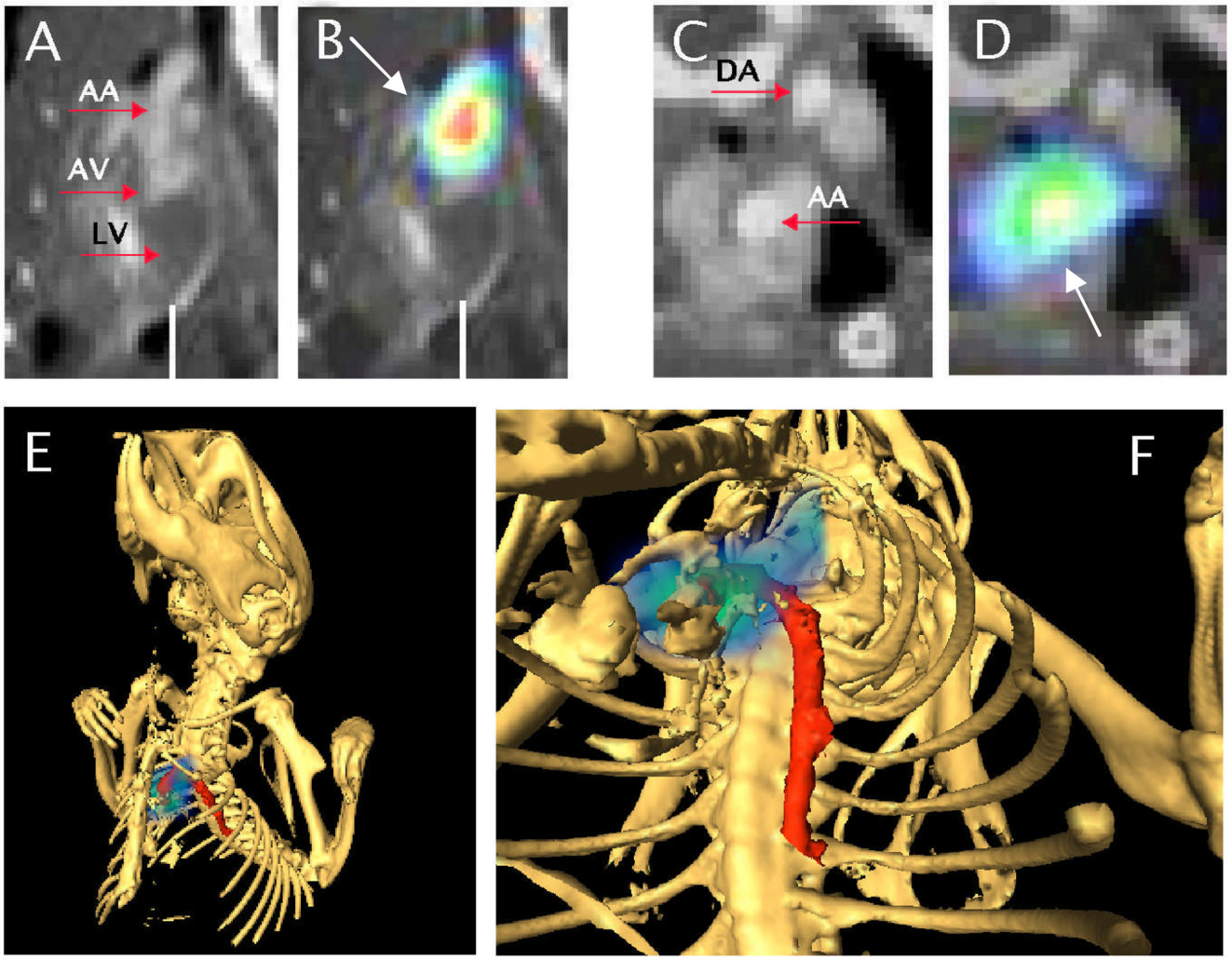

Figure 3. Magnification and 3D view of the SPECT/CT data shown in Fig.2 (monocytes transferred into ApoE−/− mouse)

A and **C** depict CT data only, **B** and **D** SPECT/CT overlay. **A** and **B** show sagittal views of the heart (LV = left ventricle; AV = aortic valve region) and ascending aorta (AA). Note the SPECT signal (white arrows) indicating monocyte recruitment to the ascending aorta in B. **C** and **D** depict axial views of ascending (AA) and descending aorta (DA). Note the SPECT signal in D in the ascending aorta, correlating with the location in B. **E** and **F**, 3D rendering; bony structures rendered in white, aorta in red and monocyte recruitment in blue-green scale. See also web-movie for animation of 3D-dataset.

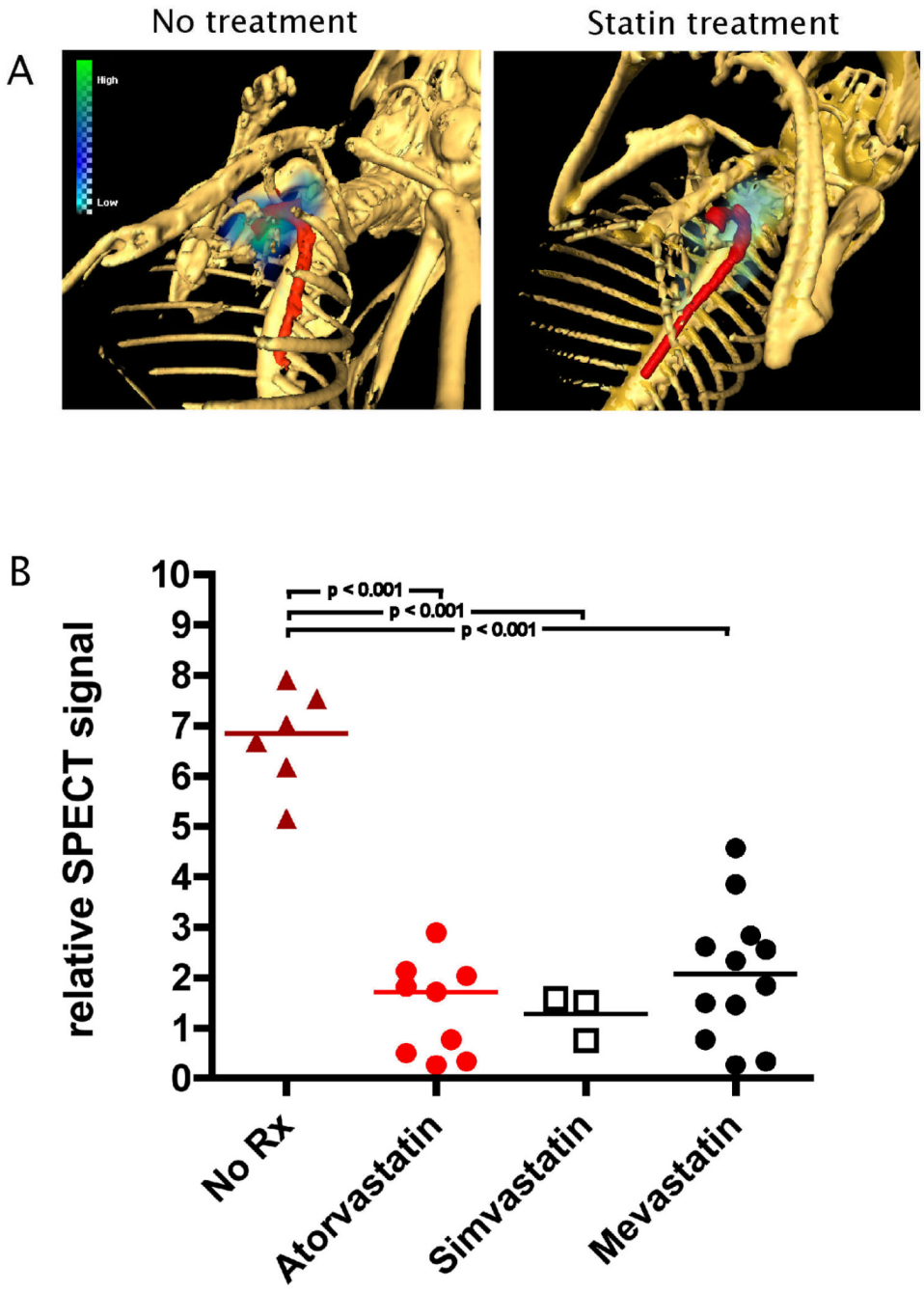

Figure 4. MicroSPECT/CT imaging allows noninvasive assessment of treatment effect of statins drugs on monocyte recruitment

A, Representative example of *in vivo* imaging of statin treatment. Note the absent activity in the aorta in the animal treated with atorvastatin. Skeleton rendered in white, aorta in red and monocyte recruitment in blue-green scale.

B, Differences of *in vivo* recruitment between placebo-treated animals (no Rx) and animals treated with different statins. Statistics (p-value) for each group were calculated by using one-way ANOVA with Tukey's multiple-comparison test.

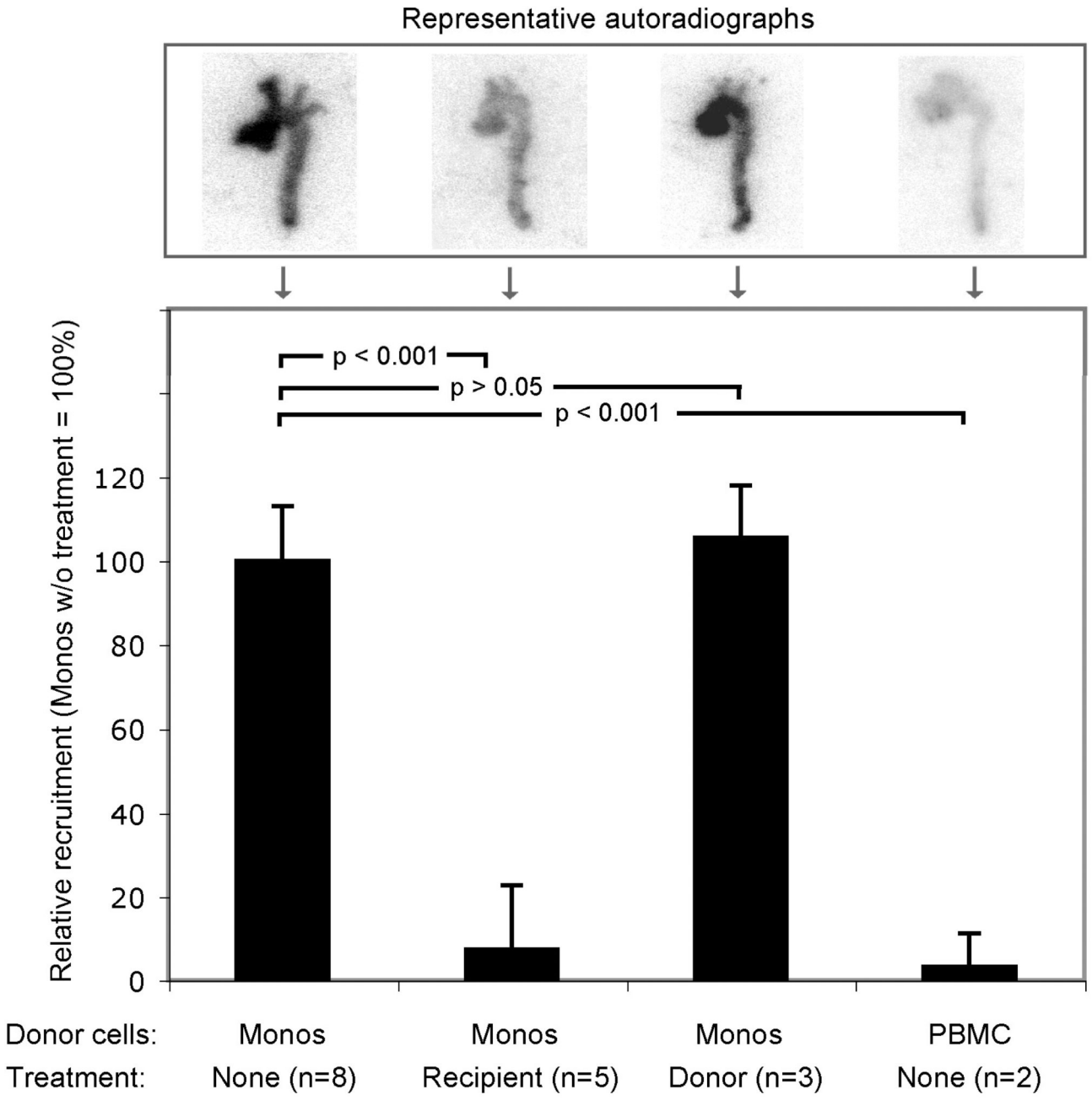

Figure 5. Ex vivo quantification of atorvastatin treatment effect on monocyte recruitment

Adoptive transfer experiments were performed either without treatment or with atorvastatin treatment of recipient or donor mice, respectively. Excised aortas were exposed on autoradiography plates and quantitative analysis of radioactivity performed. Results were expressed as relative recruitment of cells (monocytes without treatment scaled to 100%). Statistics (p-value) for each group were calculated by using one-way ANOVA with Tukey's multiple-comparison test.